High capacity variable friction damper based on band brake technology

Austin Downey [a],*, Liang Cao [a], Simon Laflamme [a], Douglas Taylor [b], James Ricles [c]

[a] Department of Civil, Construction, and Environmental Engineering, Iowa State University, Ames, IA 50011, USA
[b] Taylor Devices, North Tonawanda, NY 14120, USA
[c] Department of Civil and Environmental Engineering, Lehigh University, Bethlehem, PA 18015, USA

A B S T R A C T

Implementation of high performance controllable damping devices can ameliorate cost-effectiveness of structural systems for mitigation of natural hazards. However, the applications of these damping systems are limited due to a lack of (1) mechanical robustness; (2) electrical reliability; and (3) large resisting force capability. To broaden the implementation of modern damping systems, a novel semi-active damping device is proposed. The device, termed Banded Rotary Friction Device (BRFD), has enhanced applicability compared to other proposed damping systems due to its cost-effectiveness, high damping performance, mechanical robustness, and technological simplicity. Its mechanical principle is based on a band brake, which results in a high amplification of the applied force while enabling a variable control force. The theoretical model of the BRFD is presented and experimentally verified by subjecting a prototype to various harmonic loads. Results show that the prototype BRFD is capable of a maximum force of 45 kN (10 kips) using only a 267 N (60 lb) actuation force, therefore providing a mechanical advantage of 169. A 3-stage dynamic model previously developed by the authors can successfully be used to model the dynamic behavior of the BRFD.

© 2016 Elsevier Ltd. All rights reserved.

1. Introduction

Passive supplemental damping devices have become widely accepted in structural engineering for natural hazard mitigation [1,2]. However, they are typically only applicable to a limited bandwidth of excitations because their damping forces cannot be varied post manufacturing. Active dampers are possible alternatives to provide higher mitigation performance. Nevertheless, they require large external power sources that may not be available during or after a natural hazard, have the potential to destabilize a system, and can be expensive to operate during sustained wind events [3].

Semi-active damping strategies combine some of the benefits of passive and active strategies [4]. They are purely reactive systems, in the sense that they cannot add energy to the controlled system, and can alter their mechanical properties to provide additional controllability using a fraction of the power required by active strategies. Semi-active devices are divided into four classes: variable stiffness [5,6], variable orifices [7], variable fluid [8] and variable friction [9] devices.

In particular, variable friction devices are capable of high energy dissipation, independent of velocity by dissipating mechanical energy into heat via a friction force that is controlled by an actuator with a varying normal force. Examples of actuators used in variable friction devices include: pneumatic [10,11], hydraulic [12], electromagnetic [13,14], electro-mechanical [15,16] and piezoelectric [17–20]. This controllability of the normal force minimizes obstacles found in passive friction devices, namely, the response produced by the strong nonlinear behavior, degradation of sliding interface, and cold weld [21,2].

Literature cites several examples of working variable friction prototypes for structural control applications. A semi-active independently variable friction device possessing a 25 kN (5.5 kips) maximum damping force provided by an electromechanical actuator has been experimentally verified [15]. Others [18,22] have investigated piezoelectric friction devices (PFD) of 0.5 kN (2.2 kips) and 25 kN (5.5 kips) damping force capacity, respectively. An electromagnetic friction damper device (EFD) having a 2.84 kN (0.64 kips) damping force capacity has also been developed [23].

Despite these efforts to produce semi-active friction devices suited for structural control applications, combined with studies demonstrating their economic advantages over passive systems, (see [24–26]), their implementation has remained limited. This could be due to low damping capability and the unavailability of mechanically reliable technologies [27].

In an effort to provide both high damping capacity and high mechanical reliability, the authors have recently proposed a variable friction device based on automotive dual servo drum brake

* Corresponding author.
  E-mail address: adowney2@iastate.edu (A. Downey).

technology. The technology, termed the Modified Friction Device (MFD), was theoretically presented [28] and a prototype fabricated and demonstrated [27]. While the prototype was a small scale version constructed from a 200 mm (8 in) automotive duo-servo drum brake, a key feature found in the experimental verification was a discontinuity of the friction dynamics when the rotation reversed due to the internal layout of the braking shoes and bracing pins. This discontinuity led to a sharp reduction in the damping force provided during a substantial portion of a damping cycle. Under specific conditions of limited displacement, the damper was found to provide very limited damping force, irrespective of the applied force. The maximum damping force obtained from the prototype was 3.1 kN (0.7 kip).

The objective of this paper is to introduce a second generation of rotary variable friction devices with substantially enhanced applicability to mitigation of structural vibrations. This second generation device is designed to be capable of producing a damping force of one order of magnitude higher while overcoming the limitations found in the dynamics of the MFD and preserving a simple and mechanically robust design. This novel device, presented for the first time, is based on band brake technology, and is termed Banded Rotary Friction Device (BRFD). Band brakes have been used in mining and marine mooring applications for decades [29,30] and have proven to be a mechanically robust technology [31]. Their maintenance costs are known to be limited due to their simple mechanics, no internal parts or hydraulic fluid, and the easy replacement/availability of friction material [32]. In this paper, the BRFD is introduced, and a working prototype is experimentally verified. The 3-stage dynamic model developed by the authors [27] is used to characterize its behavior.

The paper is organized as follows. The next section introduces the BRFD and provides its theoretical background. This is followed by a presentation of a 3-stage dynamic model used in the characterization of the device's dynamic behavior. The subsequent section discusses the experimental methodology and the prototyping of the BRFD, along with a presentation and discussion of the experimental results. The last section concludes the paper by providing a summary of the findings.

2. Banded Rotary Friction Device

The BRFD utilizes existing band brake technology. A band brake is a robust and reliable friction brake consisting of a flexible band lined with friction material that tightens concentrically around a cylindrical drum to slow or stop its rotation. The BRFD is a double band brake system, consisting of a band lined with a friction material [32], doubled wrapped around a drum, as shown in Fig. 1a. It is capable of providing variable braking torques as a linear function of an applied force, which is significantly amplified by the brake's positive servo effect.

A 45 kN (10 kips) capacity prototype was fabricated based on the schematic shown in Fig. 1a. The flat double wrap band is illustrated in Fig. 1b. The band is lined with friction material and wrapped 670° around the circumference of the steel drum and anchored at both ends. The single end of the band is attached to an actuation mechanism consisting of a threaded rod for the purpose of varying the force applied to the band brake, and the double end of the band is anchored to the rigid frame. The prototype has been designed to be installed within a structural bracing scheme. Such an implementation scheme is discussed below.

2.1. Implementation within a structural system

The BRFD is designed to transform displacement into rotation, θ. The device can therefore be integrated within a multiplicity of

(a) double wrap band brake system
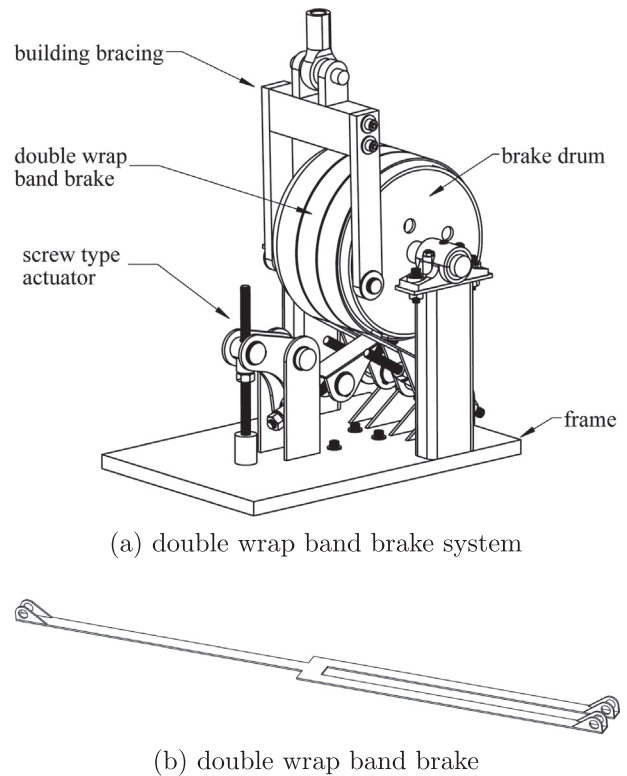

(b) double wrap band brake

Fig. 1. Banded rotary friction device.

structural control schemes, including hybrid base-isolation systems, semi-active tuned mass dampers, and bracing elements. Fig. 2 shows the BRFD installed in two possible configurations associated with a building lateral load resisting system. Fig. 2(a) is a chevron system that transduces interstory drift δ into rotation θ of the BRFD via the addition of a connecting link. Fig. 2(b) is a toggle bracing configuration. The toggle bracing is used in structural motion engineering to amplify the interstory drift [33]. While more expensive than a typical chevron system, a toggle bracing system allows the BRFD to reach a maximum frictional force faster, thus increasing the mitigation performance of the device. In both configurations the inter story drift $\delta = x/H$, where x and H are the lateral displacement of the floor and the story height, respectively. An expression for the linear displacement y can be written as

$$y = \theta \cdot r_b \tag{1}$$

where r_b is the distance from the center of the drum to the brace connection. For the chevron configuration where $y = x$ the rotation can be derived as

$$\theta = \frac{\delta \cdot H}{r_b} \tag{2}$$

For the toggle configuration, assuming small displacements, it can be shown that [34]

$$y = \frac{\sin(\alpha)}{\cos(\alpha + \beta)} \cdot x \tag{3}$$

and

$$\theta = \frac{\sin(\alpha)}{\cos(\alpha + \beta)} \frac{\delta \cdot H}{r_b} \tag{4}$$

Eqs. (2) and (4) can be used in a performance-based design procedure [3]. The following section derives the equations governing the BRFD friction mechanism.
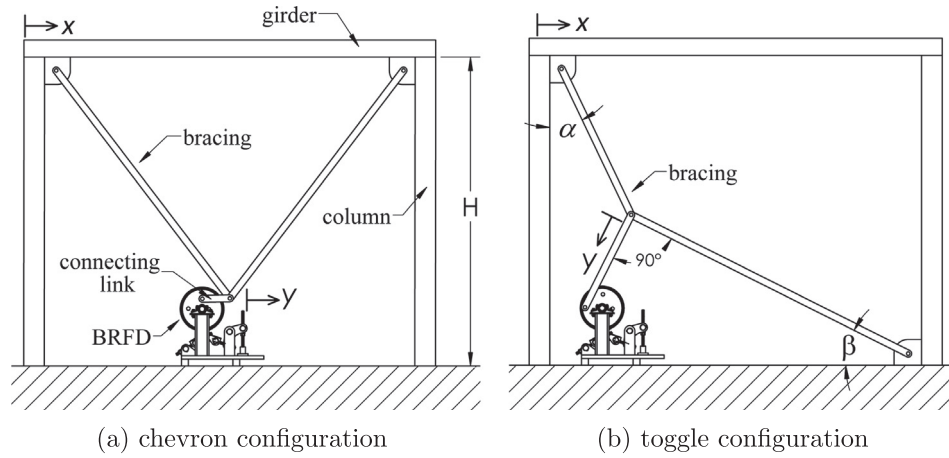
Fig. 2. Two possible configurations for the BRFD installed within a building's lateral load resisting structural system.

2.2. Friction mechanism

The friction force of the BRFD is generated by the drum rotating through the stationary band. The band is anchored at one end (called the slack end), where an input force ($F_{applied}$) is applied to the band, resulting in a reactionary force ($F_{reaction}$) at the opposite end, as shown in Fig. 3. When rotation of the drum is initiated, a friction force ($F_{friction}$) is generated opposing the rotation of the drum at the interface between the friction material and the drum. This force causes the band to experience an elastic deformation and displacement in the direction of the drum rotation. The forces present in the band are expressed as [35],

$$F_{reaction} = F_{friction} + F_{applied} \qquad (5)$$

As the tension in the band increases towards the pinned end, the band wraps tightly around the drum, creating the positive servo effect, also known as the self-energizing effect. This phenomenon increases the contact pressure of the friction material linearly with respect to the angular displacement from the point of the applied force on the drum [35]. The continuously changing contact pressure between the band and the drum is shown in Fig. 3. The contact pressure increases uniformly from p_0 to p_{max}.
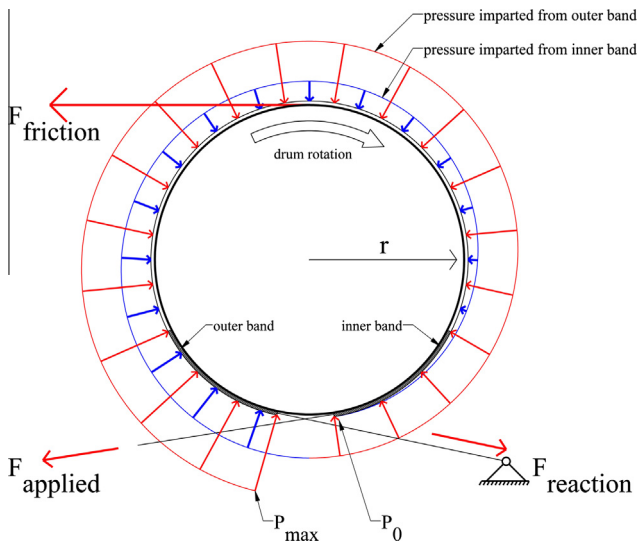

Fig. 3. Forces acting on the BRFD.

For the mathematical model it is assumed that the drum surface has a uniform curvature and the band conforms evenly to the drum surface. The initial asymmetry due to the elastic deformation of the band material is not considered. The forces $F_{applied}$, $F_{reaction}$ and $F_{friction}$ can be related to each other as follows. The relationship between the forces acting on the band ends ($F_{applied}$ and $F_{reaction}$) is expressed as

$$F_{reaction}/F_{applied} = e^{\mu\phi} \qquad (6)$$

where ϕ and μ represent the band wrap in radians and the friction coefficient of the friction material, respectively. Eqs. (5) and (6) can be combined to show

$$F_{reaction} = \frac{F_{friction} \cdot e^{\mu\phi}}{(e^{\mu\phi} - 1)} \qquad (7)$$

$$F_{applied} = \frac{F_{friction}}{(e^{\mu\phi} - 1)} \qquad (8)$$

It can be noted from Eq. (5) that the friction force $F_{friction}$ is independent of the drum radius r. However, a braking torque T can be expressed as $T = F_{friction} \cdot r$. This braking torque is used to generate a damping force, $F_{damping}$,

$$F_{damping} = \frac{T}{r_b} = \frac{F_{friction} \cdot r}{r_b} \qquad (9)$$

where $F_{damping}$ is the force applied to the bracing element. From Eq. (9), the device's mechanical advantage C is derived as:

$$C = \frac{F_{damping}}{F_{applied}} = (e^{\mu\phi} - 1) \cdot \left(\frac{r}{r_b}\right) \qquad (10)$$

where $F_{damping} > F_{applied}$ [36]. The mechanical advantage C is a function of the constants ϕ (expressed in radians), μ, r and r_b, which are determined during the device's design process. It follows that $F_{damping}$ is a linear response of $F_{applied}$ amplified by the constant C.

A schematic of the side view of the BRFD is shown in Fig. 4, where forces w_1 and w_2 can be either ($F_{applied}$) or ($F_{reaction}$) depending on the direction of rotation of the drum. This design implementation allows for the damper to take advantage of the positive servo effect in both directions of rotation. The BRFD is designed to sit on two support legs that produce opposite forces F_{leg} that counteracts the moment produced by the friction forces on the drum.
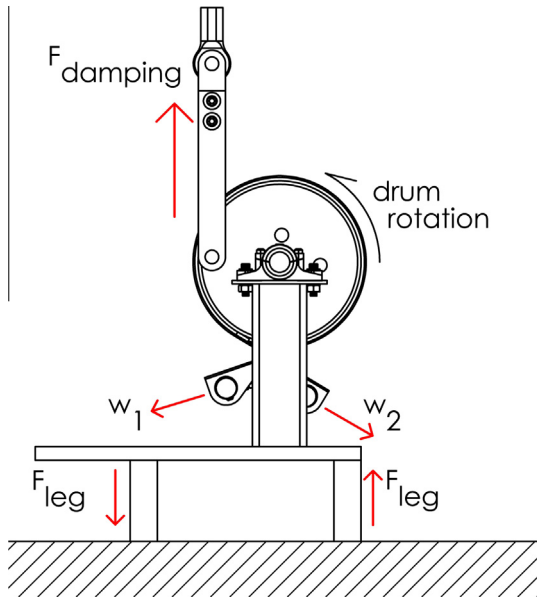
Fig. 4. Schematic of the side view of the BRFD.

3. Dynamic model

The authors have previously proposed a 3-stage dynamic model based on a modified LuGre model [27] for characterizing the friction behavior of the first generation of a rotary damping device (i.e., the MFD). This particular dynamic model was useful at characterizing the drop in force that occurs when the rotation of the drum is reversed. As it will be observed in the experimental results presented herein, the BRFD still exhibits a small drop in force upon reversal and the 3-stage dynamic model therefore still applies. This can be observed in Fig. 5 under "stage 2". This drop in the force is a product of the rearrangement of the device's components and forces caused by the change in direction of the brake drum, termed backlash. Four major sources of backlash in the BRFD prototype are as follows:

1. Elastic deformation of the band that occurs during the initial drum rotation.
2. Deviations of the band from an ideal uniform curvature encasing the drum, causing non-uniformed strain in the metal band.

3. Excess curvature present were the band connects to the supporting linkage. The curvature of the band in the connecting region changes when the force changes from ($F_{applied}$) to ($F_{reaction}$), resulting in a changing chord length. This phenomenon can be seen in Fig. 7.
4. Deflection of the base and legs supporting the rotating drum.

The 3-stage dynamic model allows for the accurate modeling of the hysteretic behavior, including the stiffness region developed by the BRFD's backlash. Fig. 5 illustrate the three different stages through a plot of a typical dynamic response of the BRFD extracted from the experimental results under a harmonic displacement input of 25.4 mm (1 in) amplitude, divided into 3 stages:

- Stage 1 (location 1 ⟶ location 2) – The system is in a typical dynamic friction mode. The friction force associated with this stage, (F_1), is characterized using a LuGre friction model. This stage occurs until rotation is reversed and the frictional force is lost.
- Stage 2 (location 2 ⟶ location 3) – The linear force F_2, associated with Stage 2 is characterized as being proportional to a stiffness element k_2. This stage occurs over a drum displacement d_2. The length of this stage is governed by the amount of backlash present in the device.
- Stage 3 (location 3 ⟶ location 1) – The force F_3 associated with this stage is characterized as being proportional to a stiffness element k_3. This stage occurs over a drum displacement d_3, after the backlash gap has been taken up by the rotating drum.

The LuGre friction model was selected to characterize the device's friction mode due to its capacity to model the stick–slip motion and the Stribeck effect [37]. The LuGre model has been applied to a wide range of systems due to its computational simplicity [38–41]. Under this model, the friction force is written

$$F_{friction} = \sigma_0 z + \sigma_1 \dot{z} + \sigma_2 \dot{\zeta} \tag{11}$$

with

$$\dot{z} = \dot{\zeta} - \sigma_0 \frac{|\dot{\zeta}|}{g(\dot{\zeta})} z \tag{12}$$

where σ_0 is a constant representing the aggregate bristle stiffness, σ_1 is the microdamping, σ_2 is the viscous friction, z is an evolutionary variable, $\dot{\zeta}$ is the BRFD's surface displacement and velocity, and $g(\dot{\zeta})$ is a function used to describe the Stribeck effect
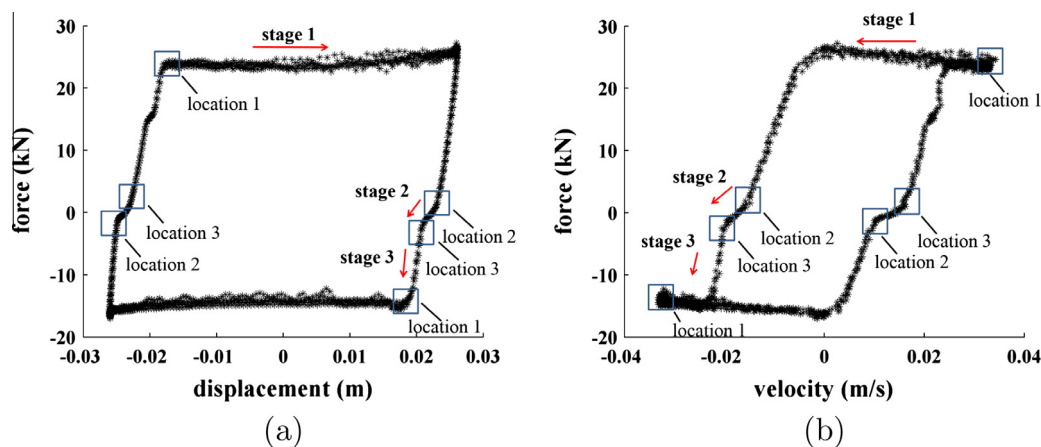

Fig. 5. Dynamic response of the BRFD under applied force of 133 N (30 lb): (a) force–displacement hysteretic response (0.2 Hz) and (b) force–velocity hysteretic response (0.2 Hz).

$$g(\dot{\zeta}) = F_c + (F_s - F_c)e^{-\left(\frac{\dot{\zeta}}{\dot{x}_s}\right)^2} \qquad (13)$$

where $\dot{x}_s$ is a constant representing the Stribeck velocity, F_s is the static friction force, and F_c the kinetic friction force. F_s is taken when the velocity of the device $\dot{\zeta} = 0$, and F_c taken as the steady state force (when $\dot{\zeta} \gg \dot{x}_s$). In Eq. (10), $\zeta \approx \theta \cdot r$.

A smoothing function is introduced to the transition region between each dynamic stage. It consists of a C^{∞} function of the following type [42]:

$$m(\zeta) = \frac{1}{1 + e^{-\frac{\gamma_1(\zeta - \zeta_0)}{\gamma_2}}} \qquad (14)$$

where ζ_0 is the reference displacement of the new stage, and γ_1, γ_2 are constants. For instance, the total force F during the transition from stage i to stage j is written

$$F = (1 - m(\zeta))F_i + m(\zeta)F_j \qquad (15)$$

where $F_{i,j}$ is the total force computed using the definition of stage i, j. Remark: the amplitude of the damping force of the prototype is not symmetric as a function of the rotational direction. This can be explained by the asymmetries in the friction material and band. A proper break-in procedure should significantly reduce or eliminate the unsymmetrical damping dynamics. This is out-of-the-scope of this paper. Here, the static and dynamic friction force coefficients are separated between forward ($F_{s,\text{fwd}}$ and $F_{c,\text{fwd}}$) and backward ($F_{s,\text{bwd}}$ and $F_{c,\text{bwd}}$) force components.

4. Experimental validation

4.1. Prototype

A prototype of the BRFD from the schematic shown in Fig. 1a was fabricated to verify its performance at producing high damping forces. Friction material used was flexible, asbestos-free, woven yarn material with copper wire [32]. The design parameters are listed in Table 1. A photograph of the prototype is shown in Fig. 6.

4.2. Methodology

The prototype BRFD was mounted in a servo-hydraulic testing machine and its characterization performed. Applied forces where controlled through a screw-activated tensioner attached to one side of the band. A load cell was placed between the BRFD's frame and the activation mechanism for measuring the applied forces. The damping force generated by the BRFD was measured via a load cell located in the head of the testing machine. The test setup is shown in Fig. 6, with the BRFD in its fully un-actuated position. The testing of the BRFD was limited to its designed 45 kN (10 kips) damping force capacity.
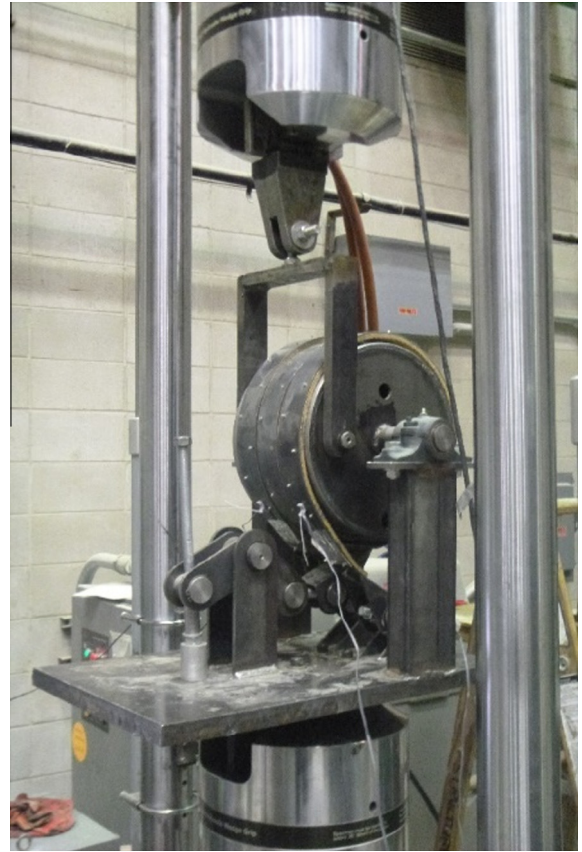

Fig. 6. BRFD testing setup.

The prototype was subjected to displacement-controlled harmonic excitations of 25.4 mm (1 in) amplitude at four different frequencies: 0.05, 0.1, 0.2, and 0.5 Hz. Five different applied forces (F_{applied}) were investigated: 35 (8), 53 (12), 66 (15), 133 (30) and 267 N (60 lbs), where 35 N (8 lbs) is the minimum force available from the actuation mechanism and 267 N (60 lbs) corresponds approximately to the prototypes maximum capacity. A total of 20 tests were performed.

4.3. Model parameters

The 3-stage dynamic model parameters were identified by minimizing the performance function J, consisting of the fitting error between the estimated force from the model $\widehat{F}_{\text{friction}}$ and experimental data F_{friction} for each test k:

$$J_k = \|\widehat{F}_{\text{friction},k} - F_{\text{friction},k}\|_2 \qquad (16)$$

where $\| \cdot \|_2$ is the 2nd Euclidean norm. This minimization was conducted in MATLAB by using the command `fminsearch` under various arbitrary (and physically realistic) initial conditions. Model

Table 1
Design parameters of the BRFD prototype.

Parameter	Value
Drum diameter	0.30 m (12 in)
Damping radius (r_b)	0.10 m (4 in)
Drum material	A-53 steel
Total band brake length	2.13 m (84 in)
Band thickness	3.2 mm (1/8 in)
Band material	A-36 steel
Friction material	Woven, asbestos-free
Coefficient of friction (μ)	0.39
Band brake wrap (ϕ)	670°
Mechanical advantage (C)	142

Table 2
Force-dependent model parameters.

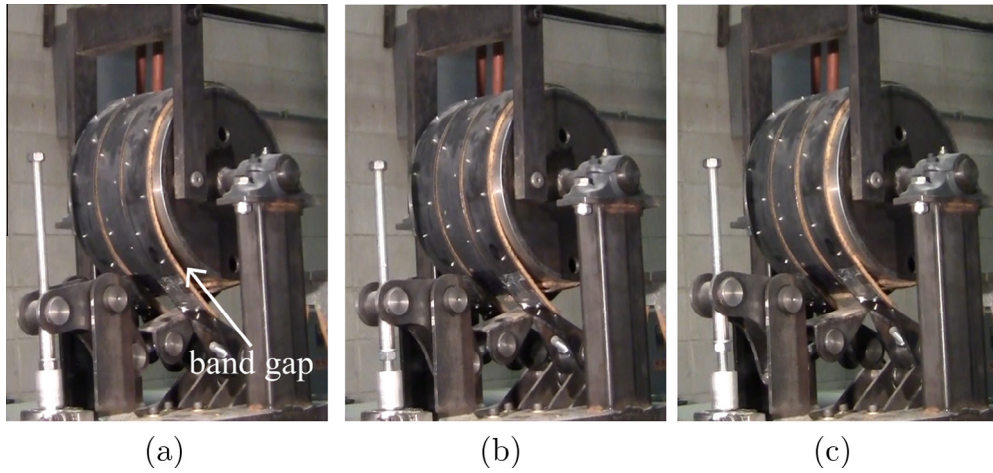| Parameter	F_{applied}				
	35 N	53 N	66 N	133 N	267 N
$F_{c,\text{fwd}}$ (kN)	0.805	1.91	13.3	22.7	37.3
$F_{c,\text{bwd}}$ (kN)	0.538	0.521	3.11	13.4	37.8
$F_{s,\text{fwd}}$ (kN)	0.894	2.23	14.2	23.6	39.1
$F_{s,\text{bwd}}$ (kN)	0.619	0.579	3.33	14.2	44.5
σ_0 (kN^{-1})	525	613	1490	5694	9198

Fig. 7. Band gap varying with the applied forces, (a) 35 N; (b) 66 N; and (c) 267 N.

Table 3
Validation of design parameters.

Parameter	Test value	Design value
C_{fwd}	145	142
C_{bwd}	126	142
μ_{fwd}	0.42	0.39
μ_{bwd}	0.41	0.39

parameters dependent on the applied force ($F_{applied}$) are the static friction F_s, the dynamic friction F_c, and the aggregate bristle stiffness σ_0.

Table 2 lists the average values of the applied force dependent model parameters, obtained from the experimental results. These average values exhibit a linear and amplified response to the applied forces. This linearity would typically be modeled and used in a model fitting task. However, due to the medium fidelity of the
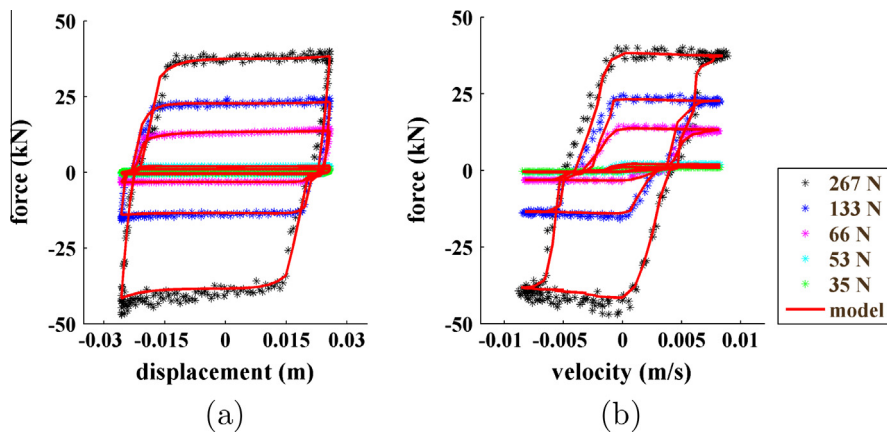

Fig. 8. Experimental data fitting under various levels of applied forces for a 0.05 Hz excitation: (a) force–displacement and (b) force–velocity plots.
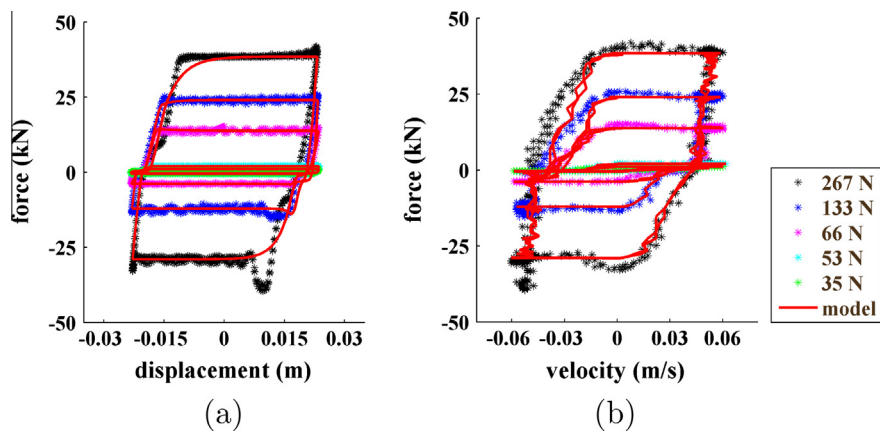

Fig. 9. Experimental data fitting under various levels of applied forces for a 0.50 Hz excitation: (a) force–displacement and (b) force–velocity plots.
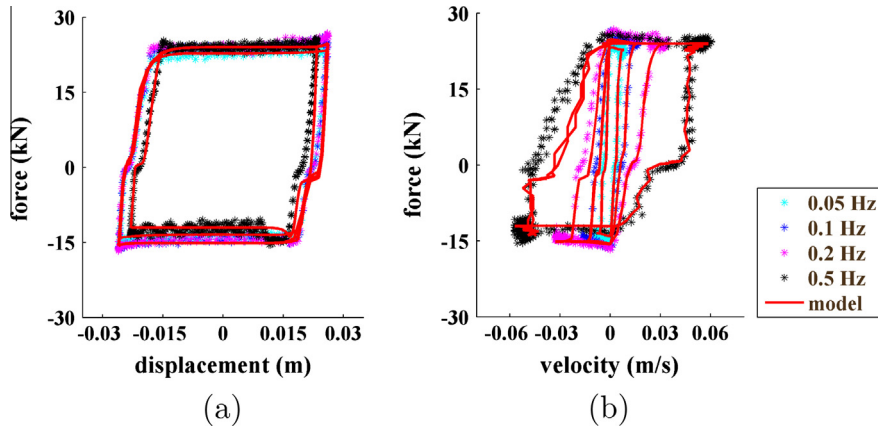
Fig. 10. Experimental data fitting under various excitation frequencies for a 133 N (30 lbs) applied force: (a) force–displacement and (b) force–velocity plots.

Table 4
Comparison of fitting RMSE (kN).

Applied force	0.05 Hz		0.1 Hz		0.2 Hz		0.5 Hz	
	3-stage	LuGre	3-stage	LuGre	3-stage	LuGre	3-stage	LuGre
35 N	5.96	15.4	6.98	13.3	8.81	21.1	14.3	29.3
53 N	3.07	5.38	3.25	5.38	3.51	6.00	3.34	5.47
66 N	4.54	44.5	2.80	40.7	2.45	55.1	4.00	100
133 N	7.56	76.3	15.7	127	44.1	46.2	27.8	117
267 N	5.56	115	9.56	58.9	12.0	40.5	22.7	126

developed prototype, test results experienced some irregularities. These irregularities are likely caused by deviations of the band from an ideal uniform curvature, and bending in the BRFD's frame. These constraints are not inherent to the devices' architecture and would be eliminated in a high fidelity prototype or production model. With the current discrepancies and the relativity low number of characterization tests performed, a linear fit of the results produces a high level of error on the estimation of the parameters. Therefore, a function of the type $F_{(c,s),(fwf,bwd)} = f(F_{applied})$ is out of the scope of this work.

(a) BRFD force-displacement

(b) BRFD force-velocity

(c) MFD force-displacement
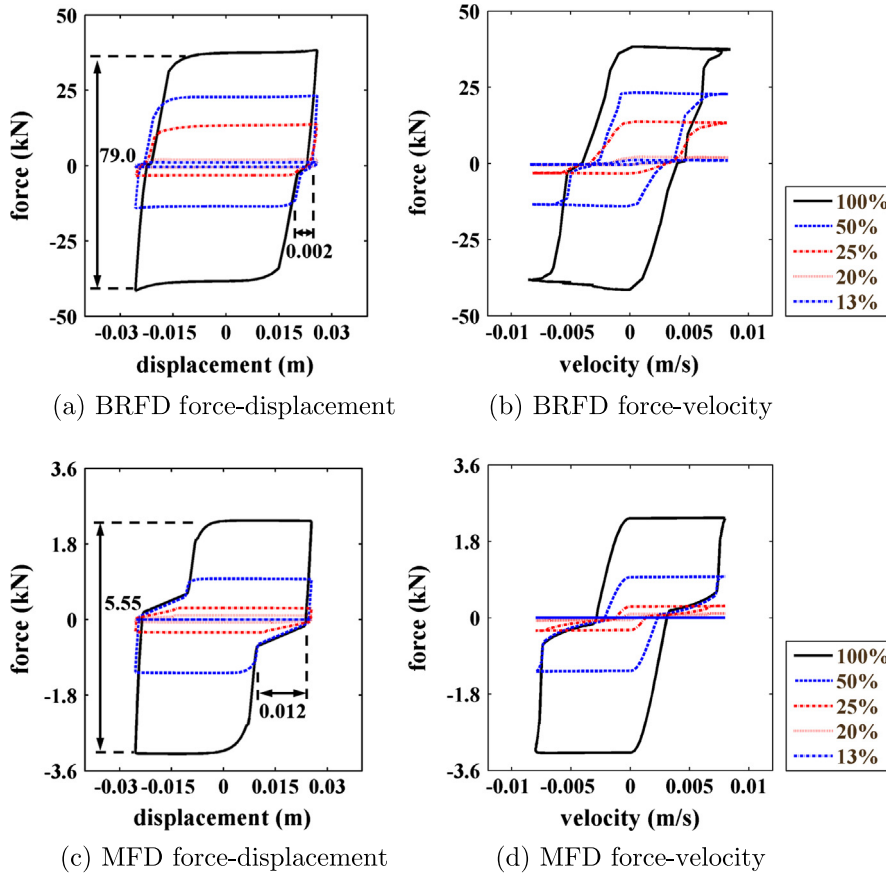
(d) MFD force-velocity

Fig. 11. Modeled dynamics of the BRFD and MFD under various applied forces under a 0.05 Hz excitation of 25.4 mm (1 in) amplitude.

The mechanical advantage C can be directly calculated by using F_c values from Table 2 as $F_{damping}$ in Eq. (10). However, given the variability in the data explained above, there would be an important variability in the experimental C computed for each test. To serve as a preliminary comparison with theory, it is best to use the values at the highest level of the applied forces, for which the band brake is the tightest and its angle is the most constant. For instance, Fig. 7 shows the changing band tension for applied forces of 35, 66, and 267 N. The change in force results in a change in the gap between the friction material on the bands and the drum, this changing distance is exhibited in Fig. 7a–c. These changes are a function of the forces applied to the band. These frames were taken while the drum was in a backwards (clockwise) rotation, where the two exterior bands are acting as the fixed or reactionary ends.

Table 3 list the C values for the forward rotation (C_{fwd}) and backward rotation (C_{bwd}) of the drum, along with the experimental friction coefficient μ derived using Eq. (10) for both rotational directions. The experimental results show an agreement with the design value of C and the materials properties provided by the manufacturer (μ). The lower C value for the backward rotation may be attributed to the asymmetries in the metal band and the adhered friction material.

4.4. Assessment of model accuracy

Figs. 8 and 9 show plots of the experimental data fitting with the 3-stage model for 0.05 and 0.50 Hz excitations, respectively,

under various levels of $F_{applied}$ (35, 53, 66, 133, and 267 N). The model shows good agreement with the experimental data for all of the applied forces. There is a loss in fitting performance at the higher frequencies due to chattering in the device. Another observation in the 0.50 Hz excitation data is an unmodeled hump that occurs with a change in the rotational direction of the brake drum, for the case of a maximum applied force (267 N), and is less apparent at 133 N. This hump is likely due to slippage of the friction material due to deviations in the brake band. Fig. 10 compares the responses under various excitation frequencies under a 133 N applied force. Results are typical of other applied forces. The model shows good agreement with the experiment data for all frequencies, with a decrease in the fitting performance at the larger frequencies. This is consistent with the previous results.

Table 4 reports the root mean square error (RMSE) between the model prediction and experimental data results. Results are also compared with a pure LuGre friction model optimized following a similar methodology used to identify the parameters for the 3-stage dynamic model. The listed RMSE confirm the performance of the 3-stage dynamic model discussed above. The pure LuGre model shows similar performance under a 53 N (12 lbs), with a substantially worst performance in the fitting to the experimental data for higher applied forces. This comparison demonstrates the necessity to still use the 3-stage dynamic model to characterize the behavior of the BRFD, due to the device's backlash.

Finally, a comparison is made between the hysteretic behavior of the first generation MFD and the BRFD. Fig. 11a and b shows the modeled force–displacement and force–velocity plots of the
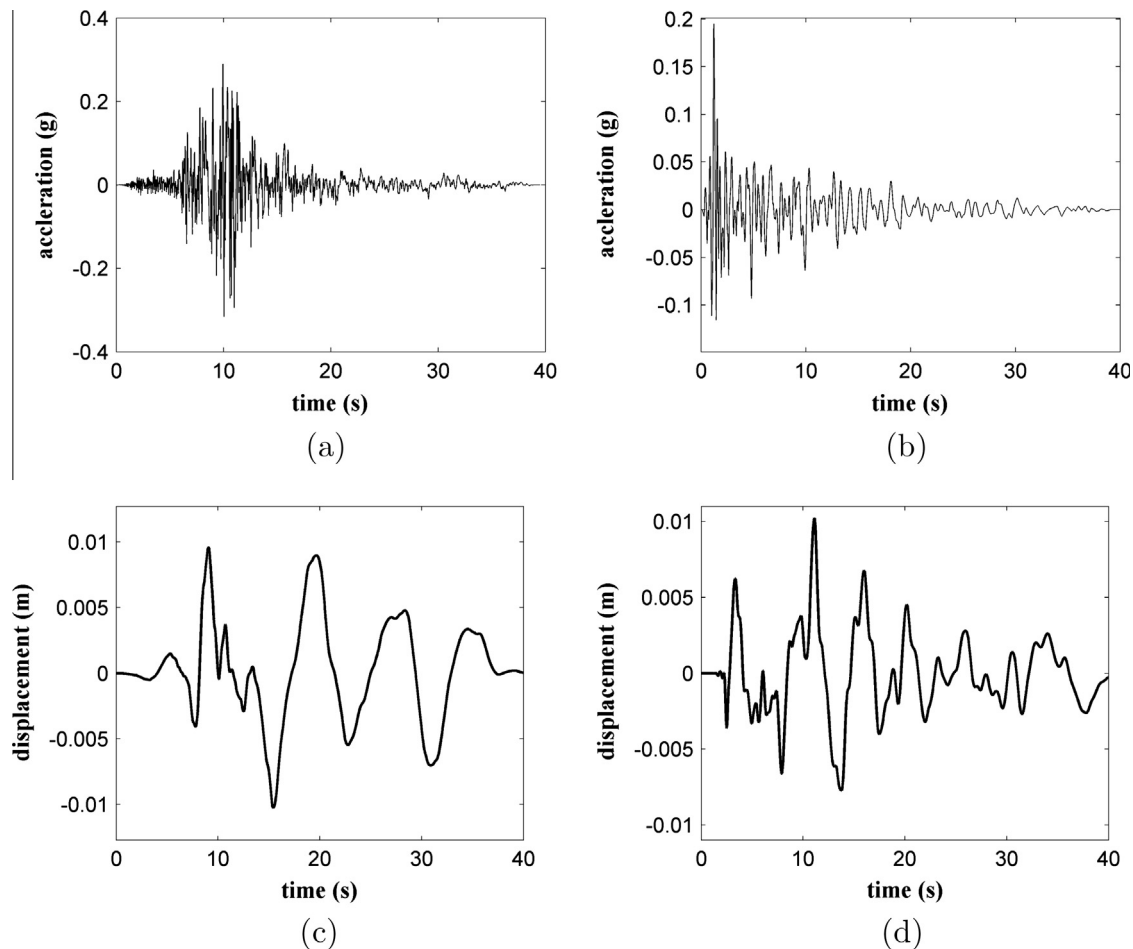

Fig. 12. Earthquake excitations: (a) unscaled ground acceleration (Imperial Valley earthquake); (b) unscaled ground acceleration (Hollister earthquake); (c) scaled ground displacement (Imperial Valley earthquake); and (d) scaled ground displacement (Hollister earthquake).

BRFD in terms of % force, starting with an applied force of 35 N (13%). For completeness, results from various applied forces are compared against the modeled dynamic behavior of the first-generation rotary damping system (the MFD) in Fig. 11c and d. The backlash region is indicated in Fig. 11a and c, along with the dynamic range under its maximum applied force. The backlash of the BRFD is reduced to 2 mm, from 12 mm for the MFD, while the dynamic range is increased from 5.55 kN (MFD) to 79.0 kN (BRFD). This demonstrates that the backlash effect has been substantially minimized, and that the BRFD is capable of producing substantially higher damping force.

4.5. Validation under nonstationary excitations

The BRFD and its model are further validated using nonstationary excitations, consisting of two seismic excitations. The first excitation is the 1979 Imperial Valley earthquake record from USGS Station 5115 and the second the 1961 Hollister earthquake record from USGS station 1028. Ground displacements were computed by double integrating the ground acceleration obtained from the PEER ground motion database [43], and the maximum amplitude of each ground displacements is scaled to 0.01 m (0.4 in) to match the testing equipment's limitations. The BRFD was subjected directly to these displacement time-histories, as the purpose of the tests was to validate the model under nonstationary dynamics rather than validating damping characteristics within a structural system. Acceleration and scaled displacement time histories are shown in Fig. 12.

The device is tested under two applied forces: 66 N (15 lb) and 133 N (30 lb). Figs. 13–16 show the time history, force–displace-

ment, and force–velocity plots for each seismic excitation. There is a good match of the theoretical model with the experimental data for both applied forces. A matching discrepancy is clearly observable under the Hollister earthquake at around 25 s (Figs. 15 (a) and 16(a)). This is due to linear approximation of the damping force during a change in the rotational direction of the drum where backlash is present. This overshoot is also present in the Imperial Valley response, and can be observed at a small magnitude at around 14 s. This phenomenon will require further investigation, but its effect could be reduced through the production of a high fidelity prototype. Results from this section demonstrate that the BRFD behaves as designed under nonstationary excitations.

5. Summary and conclusions

In this paper, a novel variable friction damper for structural control applications was presented. The device, termed Banded Rotary Friction Device (BRFD), is based on the well-accepted and mature band brake technology. This makes the BRFD a mechanically robust, semi-active damping system. It is capable of providing large damping forces with a substantially lower applied force due to its positive servo effect.

A prototype of the BRFD was fabricated and experimentally validated. The dynamic tests were conducted under harmonic loads at different frequencies and applied forces. Results show that the prototype BRFD is capable of producing a maximum 45 kN (10 kips) damping force. A 3-stage dynamic model was introduced and model parameters were identified based on test results. Results show that the model could be used to accurately characterize the
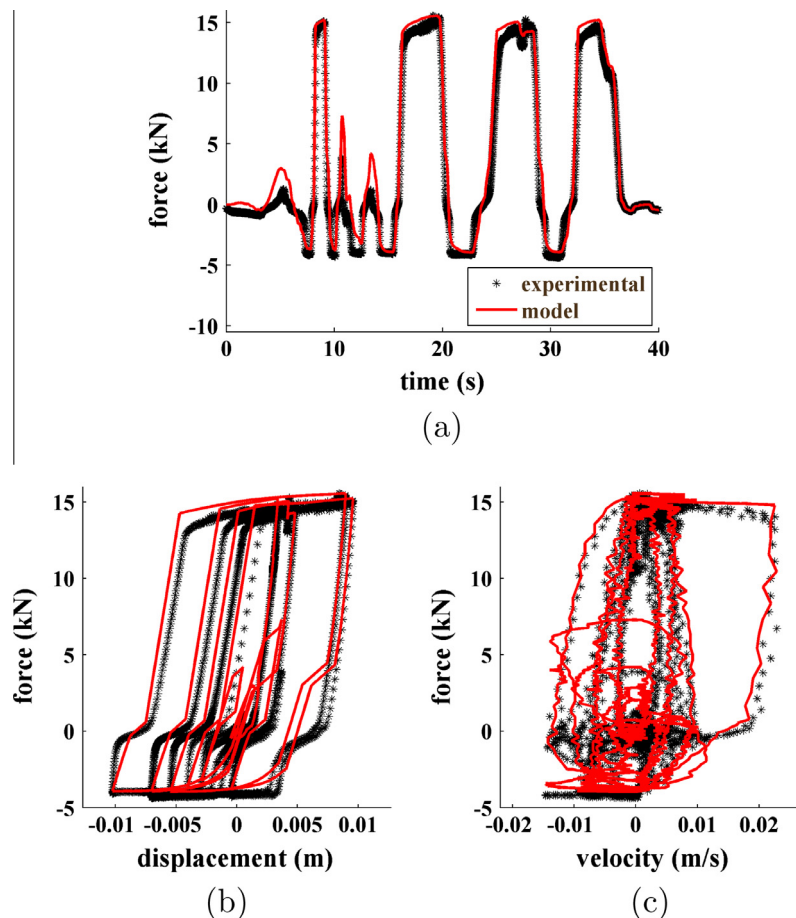

Fig. 13. Imperial Valley earthquake at 66 N (15 lb): (a) time history of damping force; (b) force–displacement loop; and (c) force–velocity loop.
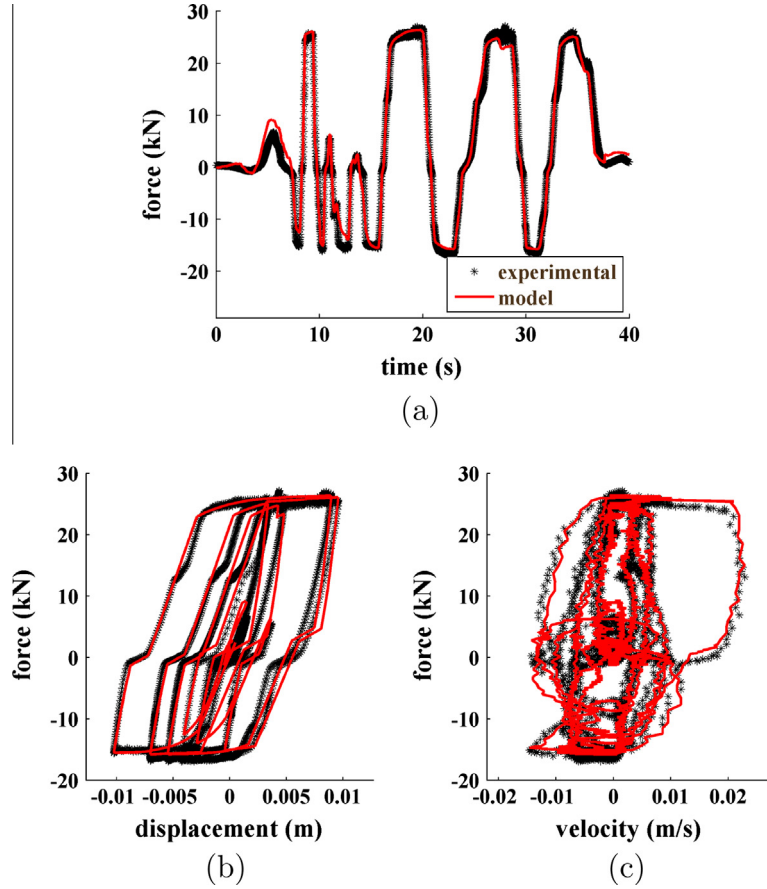
Fig. 14. Imperial Valley earthquake at 133 N (30 lb): (a) time history of damping force; (b) force–displacement loop; and (c) force–velocity loop.
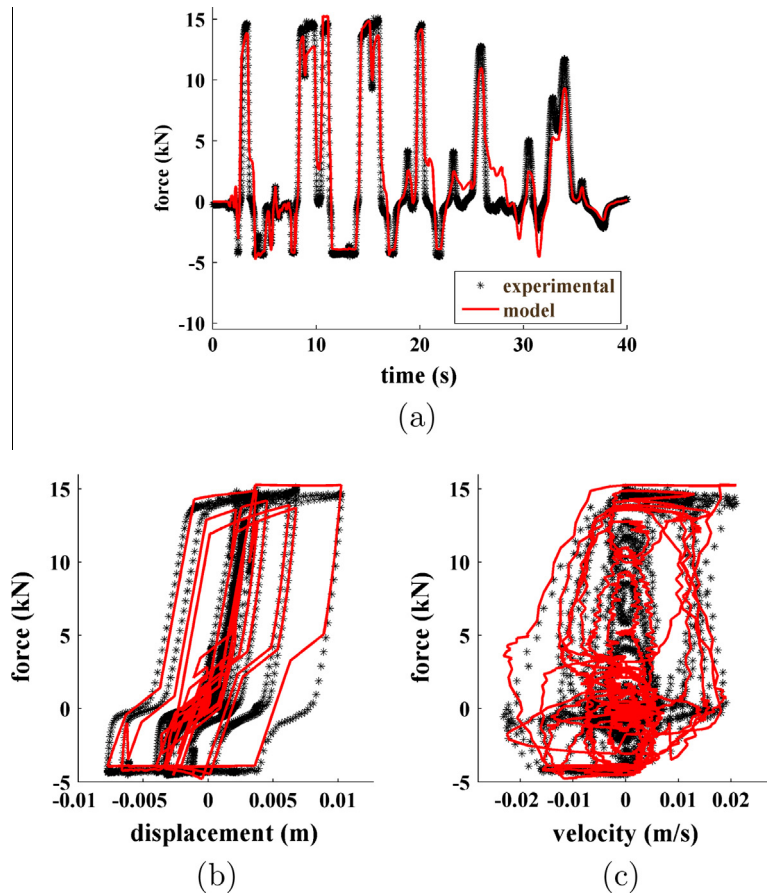

Fig. 15. Hollister earthquake at 66 N (15 lb): (a) time history of damping force; (b) force–displacement loop; and (c) force–velocity loop.
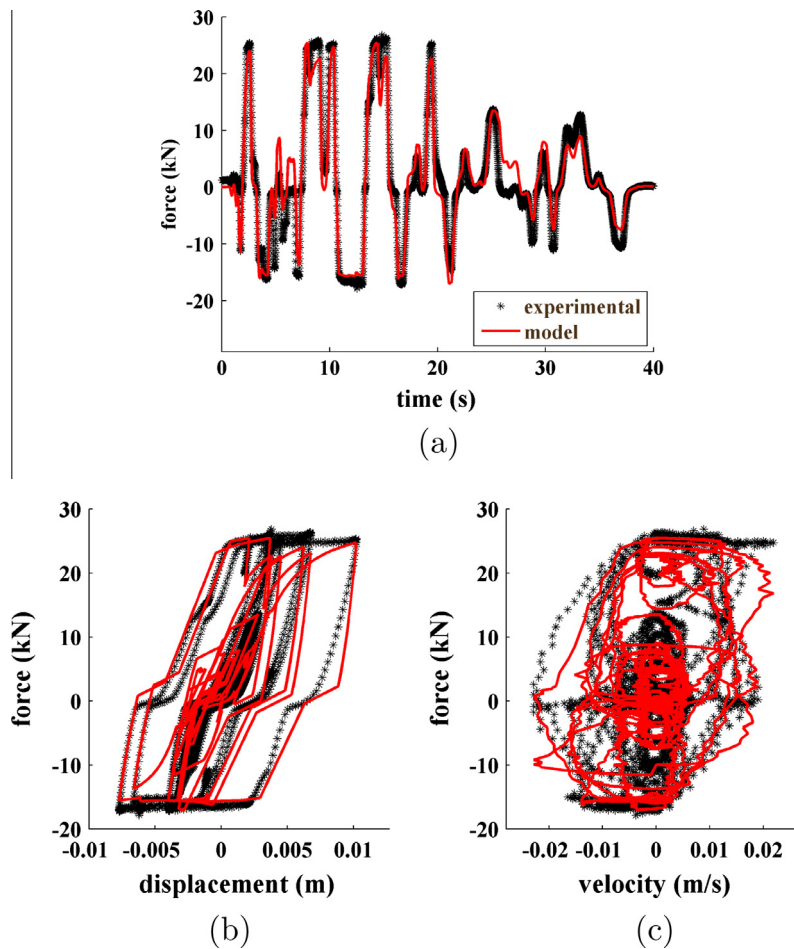
Fig. 16. Hollister earthquake at 133 N (30 lb): (a) time history of damping force; (b) force–displacement loop; and (c) force–velocity loop.

dynamic behavior of the device. The experimental mechanical advantage demonstrates that the device was capable of a force amplification in the range of 125–150 times the applied force. These numbers show agreement with theoretical values. The proposed device and its model are further validated using nonstationary excitations consisting of two earthquake time series. Results demonstrated that the BRFD behaves as designed under nonstationary excitations.

The validated prototype and friction model presented in this research advances the potential for the implementation of semi-active friction devices. The BRFD is the second generation of rotary damping systems designed by the authors. It was specifically engineered to minimize the backlash effect and increase the maximum damping force by one order of magnitude. Results showed that the BRFD's has been successful at attaining both objectives, therefore making it a mechanically robust device capable of high variable friction force.

Acknowledgements

References

[1] Spencer Jr B, Nagarajaiah S. State of the art of structural control. J Struct Eng 2003.

[2] Symans M, Charney F, Whittaker A, Constantinou M, Kircher C, Johnson M, McNamara R. Energy dissipation systems for seismic applications: current practice and recent developments. J Struct Eng 2008;134:3–21.

[3] Connor JJ, Laflamme S. Structural motion engineering. Springer; 2014.

[4] Saaed TE, Nikolakopoulos G, Jonasson J-E, Hedlund H. A state-of-the-art review of structural control systems. J Vib Control 2015;21:919–37.

[5] Liu Y, Matsuhisa H, Utsuno H. Semi-active vibration isolation system with variable stiffness and damping control. J Sound Vib 2008;313:16–28.

[6] He W, Agrawal A, Mahmoud K. Control of seismically excited cable-stayed bridge using resetting semiactive stiffness dampers. J Bridge Eng 2001;6:376–84.

[7] Yang J, Bobrow J, Jabbari F, Leavitt J, Cheng C, Lin P. Full-scale experimental verification of resetable semi-active stiffness dampers. Earthq Eng Struct Dynam 2007;36:1255–73.

[8] Yoshida O, Dyke SJ. Seismic control of a nonlinear benchmark building using smart dampers. J Eng Mech 2004;130:386–92.

[9] Spencer Jr B, Nagarajaiah S. State of the art of structural control. J Struct Eng 2003;129:845–56.

[10] Vesselenyi T, Dzitac S, Dzitac I, Manolescu M-J. Fuzzy and neural controllers for a pneumatic actuator. Int J Comp, Commun Control 2007;2:375–87.

[11] Mehmood A, Laghrouche S, El Bagdouri M. Modeling identification and simulation of pneumatic actuator for VGT system. Sens Actuat A: Phys 2011;165:367–78.

[12] Kannan S, Uras HM, Aktan HM. Active control of building seismic response by energy dissipation. Earthq Eng Struct Dynam 1995;24:747–59.

[13] Lorenz M, Heimann B, Härtel V. A novel engine mount with semi-active dry friction damping. Shock Vib 2006;13:559–71.

[14] Yang JN, Agrawal AK. Semi-active hybrid control systems for nonlinear buildings against near-field earthquakes. Eng Struct 2002;24:271–80.

[15] Narasimhan S, Nagarajaiah S. Smart base isolated buildings with variable friction systems: H controller and saivf device. Earthq Eng Struct Dynam 2006;35:921–42.

[16] Kawamoto Y, Suda Y, Inoue H, Kondo T. Electro-mechanical suspension system considering energy consumption and vehicle manoeuvre. Veh Syst Dynam 2008;46:1053–63.

[17] Chen C, Chen G. Shake table tests of a quarter-scale three-storey building model with piezoelectric friction dampers. Struct Control Health Monitor 2004;11:239–57.

[18] Lu L-Y, Lin G-L. A theoretical study on piezoelectric smart isolation system for seismic protection of equipment in near-fault areas. J Intell Mater Syst Struct 2009;20:217–32.

[19] Durmaz O, Clark WW, Bennett DS, Paine JS, Samuelson MN. Experimental and analytical studies of a novel semi-active piezoelectric coulomb damper. In: SPIE's 9th annual international symposium on smart structures and materials. International Society for Optics and Photonics; 2002. p. 258–73.

[20] Xu Y, Ng C. Seismic protection of a building complex using variable friction damper: experimental investigation. J Eng Mech 2008;134:637–49.

[21] Mualla IH, Belev B. Performance of steel frames with a new friction damper device under earthquake excitation. Eng Struct 2002;24:365–71.

[22] Pardo-Varela J, Llera J. A semi-active piezoelectric friction damper. Earthq Eng Struct Dynam 2015;44:333–54.

[23] Dai H, Liu Z, Wang W. Structural passive control on electromagnetic friction energy dissipation device. Thin-Wall Struct 2012;58:1–8.

[24] Laflamme S, et al. Control of large-scale structures with large uncertainties, Ph. D. thesis. Massachusetts Institute of Technology; 2011.

[25] Karavasilis TL, Sause R, Ricles JM. Seismic design and evaluation of steel moment-resisting frames with compressed elastomer dampers. Earthq Eng Struct Dynam 2012;41:411–29.

[26] Chae Y, Ricles JM, Sause R. Modeling of a large-scale magneto-rheological damper for seismic hazard mitigation. Part i: passive mode. Earthq Eng Struct Dynam 2013;42:669–85.

[27] Cao L, Downey A, Laflamme S, Taylor D, Ricles J. Variable friction device for structural control based on duo-servo vehicle brake: Modeling and experimental validation. J Sound Vib 2015.

[28] Laflamme S, Taylor D, Abdellaoui Maane M, Connor JJ. Modified friction device for control of large-scale systems. Struct Control Health Monitor 2012;19:548–64. http://dx.doi.org/10.1002/stc.454.

[29] Rauscher, Winch; 1922. US Patent 1413292.

[30] Johnson CA, Lucker LH, Jr. Mooring apparatus for floating vessels; 1984. US Patent 4446807.

[31] Han DS, Han GJ, Choi DH. A study on durability enhancement of band brake for mooring winch. Advanced materials research, vol. 201. Trans Tech Publ; 2011. p. 314–7.

[32] B.R.E.G. Co., Data sheet: Bermskerl 4500, 1640 Shanahan Drive, South Elgin, IL 60177; 2013.

[33] Taylor DP. Toggle brace dampers: a new concept for structural control. In: Proceedings of advanced technology in structural engineering: 2000 structures congress and exposition; 2000.

[34] Constantinou MC, Tsopelas P, Hammel W, Sigaher AN. Toggle-brace-damper seismic energy dissipation systems. J Struct Eng 2001;127:105–12.

[35] Baker AK. Industrial brake and clutch design. Pentech Press; 1992.

[36] Avallone EA, Baumeister T, Sadegh AM. Marks' standard handbook for mechanical engineers, vol. 9. New York: McGraw-Hill; 1996.

[37] Olsson H, Åström KJ, Canudas de Wit C, Gäfvert M, Lischinsky P. Friction models and friction compensation. Euro J Control 1998;4:176–95.

[38] Altpeter F. Friction modeling, identification and compensation; 1999.

[39] De Wit CC, Lischinsky P. Adaptive friction compensation with partially known dynamic friction model. Int J Adapt Control Sig Process 1998:65–80.

[40] Shiriaev A, Robertsson A, Johansson R. Friction compensation for passive systems based on the Lugre model. In: Lagrangian and Hamiltonian methods for nonlinear control 2003: a proceedings volume from the 2nd IFAC workshop. Seville (Spain): Elsevier; 2003. p. 159.

[41] Lischinsky P, Canudas-de Wit C, Morel G. Friction compensation for an industrial hydraulic robot. IEEE Control Syst 1999;19:25–32.

[42] Laflamme S, Slotine J, Connor J. Wavelet network for semi-active control. J Eng Mech 2011;137:462–74.

[43] PEER. Peer, pacific earthquake engineering research center; 2010.